Applied Sensor Fault Detection, Identification and Data Reconstruction Based on PCA and SOMNN for Industrial Systems

YU ZHANG*, CHRIS BINGHAM, MICHAEL GALLIMORE, ZHIJING YANG, JILL STEWART
School of Engineering,
University of Lincoln,
Lincoln, LN6 7TS,
U.K.
* yzhang@lincoln.ac.uk

Abstract: - The paper presents two readily implementable approaches for Sensor Fault Detection, Identification (SFD/I) and faulted sensor data reconstruction, in complex systems. Specifically, Principal Component Analysis (PCA) and Self-Organizing Map Neural Networks (SOMNNs) are demonstrated for use on industrial turbine systems. In the first approach, Squared Prediction Error (SPE) based on the PCA residual space is used for SFD, and a SPE contribution plot is employed for SFI. Furthermore, a missing value approach using an extension of PCA is applied for faulted sensor data reconstruction. In the second approach, SFD is performed by SOMNN based Estimation Error (EE), and SFI is achieved through an EE contribution plot. Data reconstruction is then based on an extension of the SOMNN algorithm. The performance of both approaches is demonstrated through use of experimental data during the commissioning of an industrial gas turbine in the sub 15MW range.

Key-Words: - Sensor fault detection and identification, Principal component analysis, Self-organizing map neural network, Data reconstruction.

1 Introduction

Sensor Fault Detection and Identification (SFD/I) has attracted considerable recent attention due to the benefits of reducing down-time and loss of productivity, and increasing the confidence of safety, quality and reliability of systems.

With regard to previously reported techniques for SFD/I, Principal Component Analysis (PCA) and Artificial Neural Networks (ANNs) have been the most popular candidate solutions. PCA based Squared Prediction Error (SPE) is well established and extensively applied for SFD in industrial processes and power control [1-8]. However, since SPE alone cannot identify the faulty sensor within a group, additional algorithms have been developed for this purpose. For instance, a Sensor Validity Index (SVI) was introduced for SFI in [1-5]. Regarding combined SFD/I, ANN techniques based on Multi-Layer Perceptron Neural Networks (MLPNNs) and Self-Organizing Map Neural Networks (SOMNNs) have been primary candidates. MLPNNs have been compared with Support Vector Machine (SVM) methods for fault detection in rotating machinery, with the conclusion that ANN's performance was generally better than SVM in terms of 'training overhead' and robustness [9]. Furthermore, SOMNNs were used for fault detection in induction machine systems [10], with a further study in [11] indicating that SOMNNs generally provide good solutions and give better results than approaches based on MLPNNs or other radial basis function neural networks (RBFNNs).

After identifying a faulted sensor, it is possible in some circumstances to reconstruct the measurements expected from that sensor and thereby facilitate improved unit availability. Data reconstruction can be achieved by extensions of the PCA- [12] and SOMNN-based approaches [13]. In this paper, PCA and SOMNN based approaches are applied for SFD/I and data reconstruction for an industrial turbine system. The efficacy and relative merits of both methods are discussed through the use of data from experimental trials.

2 Methodologies

2.1 PCA

PCA has been extensively applied for data analysis purposes, to reduce large datasets whilst preserving 'sufficient' information contained in the original underlying signal. Here, the treatment is restricted

to a brief overview to introduce terminology and definitions that are subsequently used.

Let $\boldsymbol{X}$ be the original data matrix with a mean 0.0 and a standard deviation 1.0. $\boldsymbol{X} \subset \Re^{I \times J}$, where I rows indicate the dimensions of data, i.e. the sensors, while J columns indicate the repetition of data from the experiment, i.e. the time steps.

The associated covariance matrix, $\boldsymbol{C} \subset \Re^{I \times I}$, is then obtained from

$$\boldsymbol{C} = \frac{1}{J} \sum \boldsymbol{X}\boldsymbol{X}^T . \quad (1)$$

The eigenvectors and eigenvalues of the covariance matrix are found from

$$\boldsymbol{V}^{-1}\boldsymbol{C}\boldsymbol{V} = \boldsymbol{\Lambda}, \quad (2)$$

where $\boldsymbol{V} \subset \Re^{I \times I}$, with the I column vectors representing the I eigenvectors of $\boldsymbol{C}$, and $\boldsymbol{\Lambda} \subset \Re^{I \times I}$ is the diagonal matrix of eigenvalues of $\boldsymbol{C}$, where $\Lambda_{ij} = \lambda_k$ for $i=j=k$ with λ_k as the kth eigenvalue of $\boldsymbol{C}$, and $\Lambda_{ij} = 0$ for $i \neq j$. The eigenvectors and eigenvalues are arranged in order of decreasing eigenvalues. The cumulative sum of the variance for the i^{th} eigenvalue is calculated from

$$s_i = \sum_{j=1}^{i} \Lambda_{jj} \text{ for } i=1,2,\ldots,I. \quad (3)$$

Basis vectors are selected from a subset of the eigenvectors while achieving a high value of s on a percentage basis, e.g. $s_{threshold} = 95\%$. When

$$\frac{s_{i=P}}{\sum_{j=1}^{I} \Lambda_{jj}} \geq s_{threshold}, \quad (4)$$

then the first P columns of $\boldsymbol{V}$ are used as the basis matrix $\boldsymbol{V}_\alpha \subset \Re^{I \times P}$, with $V_{\alpha\, ij} = V_{ij}$ for $i=1,2,\ldots,I$ and $j=1,2,\ldots,P$ where $1 \leq P \leq I$.

To describe the original data in principal component space, the following relation is used:

$$\boldsymbol{Y} = \boldsymbol{V}_\alpha^T \boldsymbol{X}, \quad (5)$$

where $\boldsymbol{X} \subset \Re^{I \times P}$ is the principal component matrix, which is a representation of $\boldsymbol{X}$ after PCA, with the i^{th} row representing the i^{th} principal component.

Since $\boldsymbol{V}_\alpha$ is orthonormal, for a new input data signal $\boldsymbol{x} \in \Re^{I \times 1}$, an approximation of $\boldsymbol{x}$ is given by:

$$\hat{\boldsymbol{x}} = \boldsymbol{V}_\alpha \boldsymbol{V}_\alpha^T \boldsymbol{x}. \quad (6)$$

PCA generates a principal component sub-space and a residual sub-space. Decomposing the data matrix into two parts, the principal component estimation part, and the residual part, gives

$$\boldsymbol{x} = \hat{\boldsymbol{x}} + \boldsymbol{e}, \quad (7)$$

where the residual can be expressed as

$$\boldsymbol{e} = \left(\boldsymbol{I} - \boldsymbol{V}_\alpha \boldsymbol{V}_\alpha^T\right)\boldsymbol{x}. \quad (8)$$

2.2 SOMNN

A SOMNN is a competitive learning network. An input data vector, $\boldsymbol{x} = [x_1, x_2, ..., x_I] \in \Re^{I \times 1}$, with I variables (sensors), is associated with a reference vector, $\boldsymbol{r}_i \in \Re^{I \times 1}$, which is often randomly initiated to give each neuron a displacement vector in the input space. For each sample of $\boldsymbol{x}(t)$, $\boldsymbol{r}_w(t)$ constitutes 'the winner', by seeking the minimum distance between the input vector and the reference vector, and is calculated from:

$$\|\boldsymbol{x}(t) - \boldsymbol{r}_w(t)\| \leq \|\boldsymbol{x}(t) - \boldsymbol{r}_i(t)\| \text{ for } \forall\, i. \quad (9)$$

After obtaining a 'winner', the reference vectors are updated using:

$$\boldsymbol{r}_i(t+1) = \boldsymbol{r}_i(t) + n_{w,i}(t)\left(\boldsymbol{x}(t) - \boldsymbol{r}_i(t)\right), \quad (10)$$

where $n_{w,i}(t)$ is a neighbourhood function, which is normally chosen as Gaussian. The reference vectors are adjusted to match the training signals, in a regression process over a finite number of steps, in order to achieve the final 'self-organizing maps'.

3 Sensor Fault Detection

To provide an illustrative focus for the study, a group of six burner tip temperature sensors on an industrial gas turbine system, is studied. Fig.1 shows an example of field data from an experimental trial showing sensor faults on sensor 6. Data from the first 300 minutes are used as training data, and data from 300 to 1440 minutes are applied as testing data for both approaches.

3.1 PCA based SPE

The SPE can be obtained by the square of the predicted residual, $\boldsymbol{e}$ in (8), as follows

$$SPE(\boldsymbol{x}) = \|\boldsymbol{e}\|^2 = \boldsymbol{x}^T \left(\boldsymbol{I} - \boldsymbol{V}_\alpha \boldsymbol{V}_\alpha^T\right)\boldsymbol{x}. \quad (11)$$

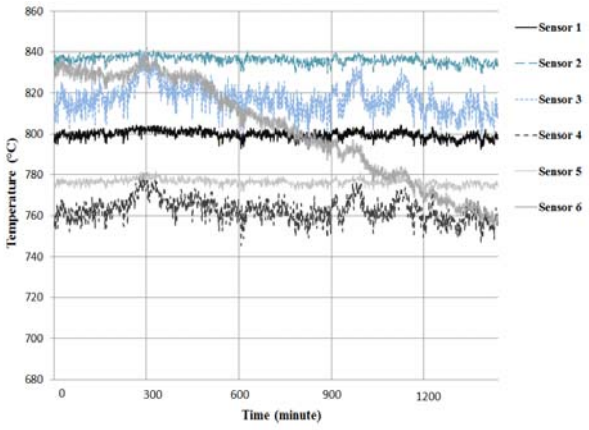

Fig. 1: Experimental trial: temperature information

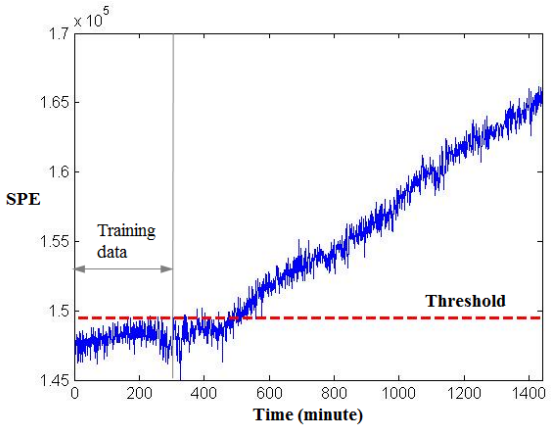

Fig. 2: Experimental trial: SPE plot

Here, the eigenvector matrix V_α is calculated from the data history matrix, in this case, the first 300 minutes, which is considered to be 'normal'.

The residuals generated by PCA are variances that cannot be modeled in principal component space. When no faults are deemed to be present, the residuals represent normal dynamics and noise in the system, in the PCA residual sub-space. In the presence of a sensor fault, there is divergence of sensor correlations, and the residual vector deviates from the normal range. In this aspect, the detection of potential sensor failures is carried out by comparing the SPE with a threshold δ_1 defined from historic data, and anomalies are deemed to occur when

$$SPE > \delta_1 . \tag{12}$$

Here, the threshold is chosen at a 95% confidence level. The SPEs are plotted in Fig.2 for the experimental trial. It is shown that abnormal conditions are detected after 500 minutes.

3.2 SOMNN based EE

SOMNN is performed using the same measurements, with 6 sensor variables and 1440 time samples in the network. To obtain a visual output of the classifications, the SOMNN is trained with the output space as 8×8 hexagonal grids, using *Matlab Neural Network Toolbox* [14]. For the training data, the weighting matrices in the component planes for the 6 sensors, are shown in Fig.3(a). For abnormal operation (data after 500 minutes), the component planes of the map are shown in Fig.3(b). It can be seen that a discrepancy exists between the weighting matrix for sensor 6 and those of the other sensors, indicating a fault on sensor 6.

To detect such effects numerically, an Estimation Error (EE) is introduced to monitor the performance of the final 'self-organizing maps':

$$EE = \left\| \boldsymbol{x}^{new} - \boldsymbol{r}_w^{new} \right\|, \tag{13}$$

which is defined as the distance between the winning weight vector $\boldsymbol{r}_w^{new}$ and the input vector $\boldsymbol{x}^{new}$ in the new state. If the EE is greater than a pre-determined percentage of the normal distribution profile, the new state signal is considered to be abnormal i.e. when

$$EE > \delta_2 . \tag{14}$$

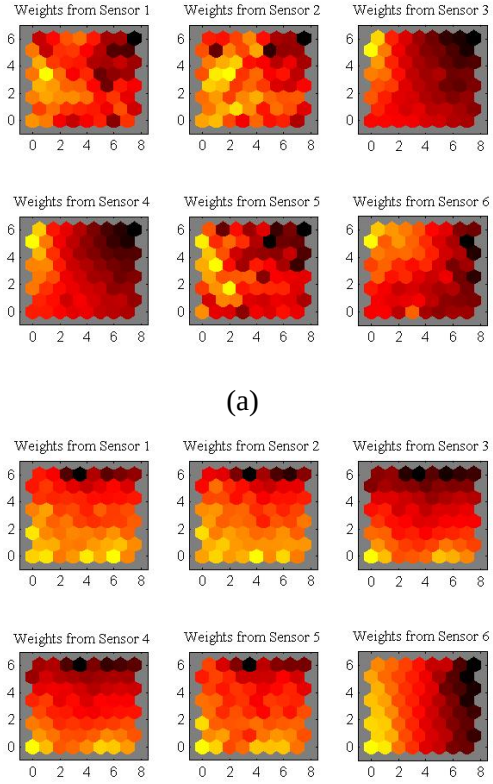

(a)

(b)

Fig. 3: Component planes of the self-organizing map: (a) normal operation, (b) faults on sensor 6

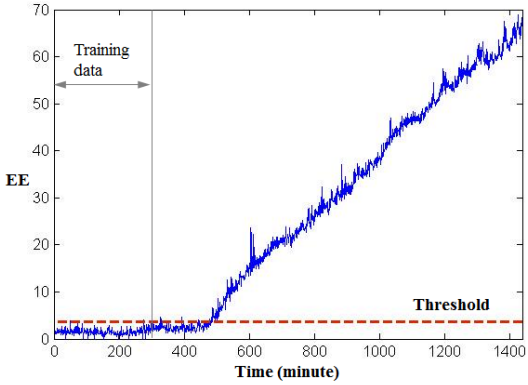

Fig. 4: Experimental trial: EE plot

The threshold is also selected as the 95% confidence level from the training data. The EE plot is shown in Fig.4 for the same experimental trial that shows fault occurring after 500 minutes. Although the error measure EE in SOMNN and the SPE in PCA are based on different algorithms, it can be seen that the results are comparable and in good agreement—see Fig.2 and Fig.4. The methods therefore provide corroborating techniques.

4 Sensor Fault Identification

SFI can be simply achieved from respective contribution plots from both PCA and SOMNN based approaches. The contribution to the SPE or EE, from each sensor, is calculated and plotted in a percentage form, in Fig.5. A greater percentage presents more error contribution from that particular sensor.

The error contribution plot is used in complement with the SPE (or EE) plots to accomplish the SFI after abnormal conditions have been detected. Again, it can be seen from both results that sensor 6 is at fault after 500 minutes.

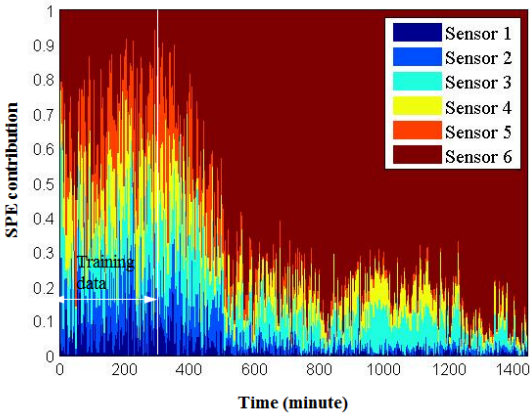

(a)

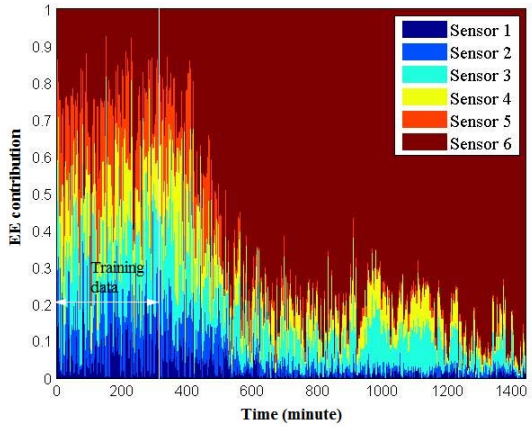

(b)

Fig. 5: Contribution plot: (a) SPE (b) EE

5 Data Reconstruction

5.1 PCA based Missing Value Approach

Following the identification of a faulted sensor, a decision needs to be made as to whether operation of the unit can continue, or whether the unit should be shut-down for immediate maintenance. The latter option often leads to enforced down-time and lost productivity. An alternative, therefore, is to try and reconstruct a 'best estimate' of the measurements expected from the faulted sensor with a view to retaining the ability to keep the unit operating.

The PCA based 'missing value' approach is now used to reconstruct the faulted signal by using the measurements from non-faulted sensors and the correlations of the sensors from the training data. Assuming the *i*th sensor is faulty, and the input signal is the original signal but without the *i*th term, then

$$\boldsymbol{x}_i = \left[\boldsymbol{x}_{-i}^T \boldsymbol{x}_{+i}^T\right]^T \in \Re^{I-1}. \tag{13}$$

The eigenvector matrix $\boldsymbol{V}_\alpha$ is modified by eliminating the *i*th row for which the *i*th sensor contributed

$$\boldsymbol{V}_i = \begin{bmatrix} \boldsymbol{V}_{-i}^T \\ \boldsymbol{V}_{+i}^T \end{bmatrix} \subset \Re^{(I-1)\times P}. \tag{14}$$

Define $\boldsymbol{\varepsilon}_i = [0\,0\ldots0\,1\,0\ldots0]^T \in \Re^I$, with the *i*th component as 1, and other components as 0s. The estimate of the faulted signal is calculated from

$$\boldsymbol{z}_i \approx \boldsymbol{\varepsilon}_i^T \boldsymbol{V}_\alpha \left(\boldsymbol{V}_i^T \boldsymbol{V}_i\right)^{-1} \boldsymbol{V}_i^T \boldsymbol{x}_i. \tag{15}$$

To evaluate the reconstruction performance, define the l_2-norm relative reconstruction error, E, as follows

$$E = \frac{\sqrt{\sum_{i=1}^{I} \| \boldsymbol{z}_i - \boldsymbol{x}_i \|_2^2}}{\sqrt{\sum_{i=1}^{I} \| \boldsymbol{x}_i \|_2^2}}. \tag{16}$$

As a test example, normal operational measurements from burner tip temperature sensors are studied, as in Fig.6. The first 1000 minutes are used as training data, and the signal for sensor 6 from 1000 to 2000 minutes, is estimated. The original and estimation signals are shown in Fig.7(a). The l_2-norm relative prediction error is 0.005% for the test example, signifying that the reconstruction bears an excellent correspondence with the 'real' measurements.

The method is subsequently applied to an experimental trial which includes the sensor failure depicted in Fig.1.

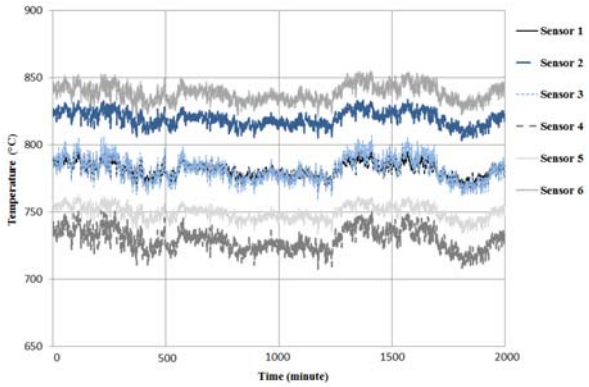

Fig. 6: Data reconstruction test example

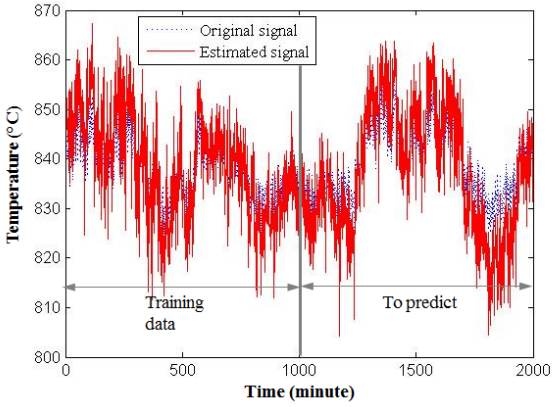

(a)

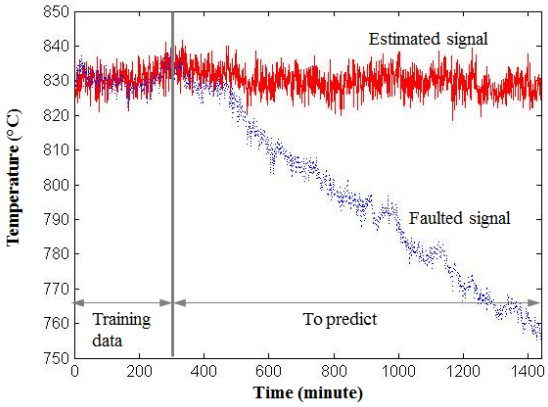

(b)

Fig. 7: Data reconstruction based on PCA: (a) test example; (b) faulted signal

The faulted signal is reconstructed as shown in Fig.7(b). It can be seen that the estimates from the training data fit well.

5.2 SOMNN based Reconstruction

Based on the SOMNN algorithm, for a 2-dimensional output space, the faulted signal can be reconstructed by adjusting the weight vector using a combination of its k nearest nodes. Firstly, a function is defined for monitoring the activation of

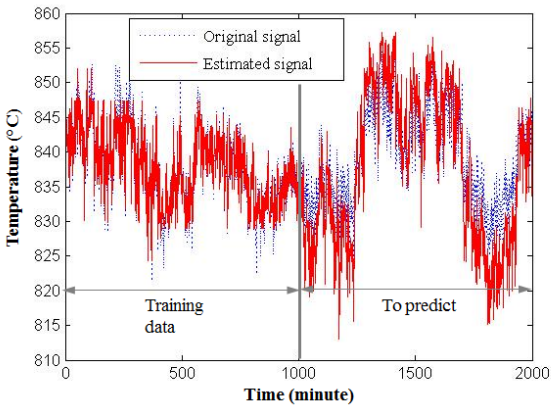

(a)

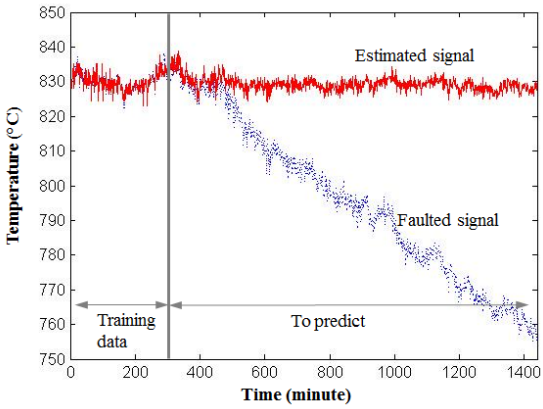

(b)

Fig. 8: Data reconstruction based on SOMNN: (a) test example; (b) faulted signal

output neuron n for an input vector $\boldsymbol{x}$ by using a Gaussian kernel:

$$T(n) = \exp\left(\frac{-1}{2\sigma_n^2}\left\|\boldsymbol{x} - \boldsymbol{r}_n\right\|^2\right), \qquad (17)$$

where σ_n^2 is a parameter representing the influence region of neuron n. When the current sample of the sensor is detected as being faulty, the winning neuron for this measurement is no longer valid, and the weighting vector is estimated by considering the k nearest neighbouring neurons of the corresponding winning neuron, in the output space, expressed as

$$z_i \approx \sum_{m=1}^{k}\left(T_m \boldsymbol{r}_{im}\right) \Big/ \sum_{m=1}^{k} T_m , \qquad (18)$$

where z_i is the estimation of the measurement, i is sensor index and m is the neuron index.

For the test example in Fig.6, the SOMNN based reconstruction result is shown in Fig.8(a). The l_2-norm relative prediction error is 0.003% in this case, demonstrating better performance of the SOMNN based data reconstruction than the PCA based method.

The technique is then applied to the experimental trial shown in Fig.1, and the signal estimation for sensor 6 is shown in Fig.8(b). From the results it can be seen that from the onset of the 'fault period', the reconstructed data follows the normal trend (given by the behaviour of the other sensors) very reliably, and could therefore be used in place of the erroneous (faulted) measurements.

It should be noted that these techniques can also be readily adapted to provide expected outputs from each sensor in a group, which can then be compared to the real-time measurements, and thereby provide a further simple mechanism for detecting unexpected characteristics.

6 Conclusion

In this paper, PCA and SOMNN based approaches are applied for SFD/I and faulted sensor data reconstruction, and there relative merits discussed. PCA based SPE and SOMNN based EE are used for SFD. Contribution plots are employed for SFI. Data reconstruction is performed through extensions of the PCA and SOMNN techniques. Both approaches are shown to be capable detecting, identifying and reconstructing data from faulted—thereby facilitating corroborative use of their attributes.

References:

[1] R. Dunia, S.J. Qin, T.F. Edgar, T.J. McAvoy. Use of Principal Component Analysis for Sensor Fault Identification. *Computers Chem. Engng*, vol. 20, 1996, pp.713-718.

[2] H.H. Yue, S.J. Qin. Reconstruction-based Fault Identification Using a Combined Index. *Ind. Eng. Chem. Res*., vol. 40, 2001, pp.4403-4414.

[3] S.W. Choi, C. Lee, J.M. Lee, J.H. Park, I.B. Lee. Fault detection and Identification of Nonlinear Processes Based on Kernal PCA. *Chemometrics and Intelligent Laboratory Systems*, vol. 75, 2005, pp.55-67.

[4] T. Xu, Q. Wang. Application of MSPCA to Sensor Fault Diagnosis. *ACTA Automatica Sinica*, vol. 32, No.3, 2006, pp.417-421.

[5] B. Lee, X. Wang. Fault Detection and Reconstruction for Micro-Satellite Power Subsystem Based on PCA. *Systems and Control in Aeronautics and Astronautics*, vol. 3, 2010, pp.1169-1173.

[6] S. Wang, F. Xiao. Detection and diagnosis of AHU Sensor Faults Using Principal Component Analysis Method. *Energy Conversion and Management*, vol. 45, 2004, pp.2667-2686.

[7] H. Liu, M.J. Kim, O.Y. Kang, S. B, J.T. Kim, C.K. Yoo. Sensor Validation for Monitoring Indoor Air Quality in a Subway Station. *Sustainable Healthy Buildings*, vol. 5, 2011, pp.477-489.

[8] J. Ni, C. Zhang, S. Yang. An Adaptive Approach Based on KPCA and SVM for Real-time Fault Diagnosis of HVCBs. *IEEE Transactions on Power Delivery*, vol. 26, No.3, 2011, pp.1960-1971.

[9] L.B. Jack, A.K. Nandi, Fault Detection Using Support Vector Machine and Artificial Neural Networks Augmented by Genetic Algorithms. *Mechanical Systems and Signal Processing*, vol. 16, No.2-3, 2002, pp. 373-390.

[10] S. Wu, T.W.S. Chow, Induction Machine Fault Detection Using SOM-based RBF Neural Networks. *IEEE Transactions on Industrial Electronics*, vol. 51, No.1, 2004, pp. 183-194.

[11] K. Elissa, L. F. Gonçalves, J. L.Bosa, T. R. Balen, M. S. Lubaszewski, E. L. Schneider, and R. V. Henriques, Fault Detection, Diagosis and Prediction in Electrical Valves using Self-organizing Maps, *Journal of Electron Test*, vol. 10, 2011, pp. 1007-1020.

[12] H. Martin, T. Naes, *Multivariate Calibration*, John Wiley and Sons, New York, 1989.

[13] T. Kohonen, *Self-Organizing Maps*, Heidelberg: Springer Verlag, 1995.

[14] Matlab version 7.10.0. Natick Massachusetts, the Mathworks Inc., 2010.